ISSN 1063-7761, Journal of Experimental and Theoretical Physics, 2021, Vol. 132, No. 5, pp. 753–765. © Pleiades Publishing, Inc., 2021.
Russian Text © The Author(s), 2021, published in Zhurnal Eksperimental'noi i Teoreticheskoi Fiziki, 2021, Vol. 159, No. 5, pp. 851–865.

ATOMS, MOLECULES, OPTICS

Influence of (0, 1)* Laguerre-Gaussian Field Distribution on Tunneling Ionization Rate

T. B. Miladinović[a,*], S. Simić[b], N. Danilović[b], and M. Z. Jeremić[c]

[a] *Institute for Information Technologies, University of Kragujevac, Jovana Cvijića bb, Kragujevac, 34000 Serbia*
[b] *Faculty of Science, University of Kragujevac, Radoja Domanovića 12, Kragujevac, 34000 Serbia*
[c] *Clinical Center Kragujevac, Department of Nuclear Medicine, Zmaj Jovina 30, Kragujevac, 34000 Serbia*
**e-mail: tanja.miladinovic@gmail.com*

Received November 17, 2020; revised January 7, 2021; accepted January 8, 2021

Abstract—In the frame of the ADK theory, the tunneling ionization of an argon atom exposed to the light from Ti:Sapphire laser is investigated. We assume that the laser field is the radially polarized beam with donut. (0, 1)* Laguerre-Gaussian field distribution. Considering that LG (0, 1)* modes can appear with random or uniform polarization (linear, circular or elliptical), we analyzed behavior of transition rate in all three types. We computed transition rate in basic case and in the case when the initial momentum of the ejected electron is included in the equation. Also, we analyzed influence of the modified initial ionization potential of ionized electron on transition rate. In the basic case, we got what we expected but with included effect we find appearance of two transition rate peaks at a certain point of the electron's exit from the barrier.

DOI: 10.1134/S1063776121050046

1. INTRODUCTION

Laser-matter interaction has been the subject of research in many papers for more than fifty years [1–4]. One of the most significant quantum processes that occurs during this interaction is ionization, and that is why it is important to be understood well. Depending on the intensity of laser field, electron can escape via tunnel, multiphoton, above-threshold ionization (ATI) and barrier suppression ionization (BSI).

When the laser field is strong enough and it's electric field strength is comparable to the atomic field strength ($F \le F_a$, $F_a = 5 \times 10^9$ V/cm), it deforms the Coulomb potential and forms a potential barrier through which electron can tunnel. Tunneling ionization takes place very quickly, close to the maximum of the field intensity and to the place where the potential barrier is maximal suppressed by the laser field.

Tunneling of an electron through a potential barrier can be described using different theoretical approaches. Landau–Lifshitz approach for tunneling is semi-classical [5]. The Keldysh theory shows that the multiphoton and tunneling ionization are basically the same, but they are realized under different laser frequency values [6]. Keldysh parameter γ is introduced as a ratio of laser period ω and tunneling frequency ω_t, $\gamma = \omega/\omega_t$. This parameter is used to distinguish between tunneling ($\gamma \ll 1$), and multiphoton domain ($\gamma \gg 1$). Perelomov, Popov and Terent'ev (PPT) obtained exact form of the pre-exponential factor of the transition rate given in [7]. Also relying on the Keldysh theory, Ammosov, Delone and Krainov in their paper gave most commonly used formula for ionization rate for arbitrary complex atoms and atomic ions (ADK theory) [8].

As we can see, tunneling ionization process is very complex and it dependents on a number of parameters, such as the radiation frequency ω, the electric field strength of radiation F and the binding energy of the electron I_p. Some of the basic variables that include these parameters and provide important process information are the transition rate, electron energy and angular distribution. In order to analyze this process, it is also necessary to consider influence of different polarizations and spatial-temporal distributions of laser field on these variables. Linear, circular and the elliptical polarizations have been already applied [9–13], and each of them caused different values certain variables. Spatial and temporal properties of a laser beam, like Gaussian and Lorentzian, affecting the transition rate, electron energy and angular distribution [14–17]. Progression in optical technology enabled investigation of these processes with radially and azimuthally polarized optical beams. Special properties of these beams led to increased interest in their use in many areas, such as, particle trapping [18], electron acceleration [19], microscopy [20], material processing [21].

Tightly focused radially polarized beam can have a strong longitudinal electric field [22], but quality of this beam could be degraded and some of the causes

are a non-concentrically aligned beam or pumped rods axes [23]. In order to amplify the beam and correct it's degenerations can be used thermally guiding fiber [24] or step-index optical fiber [25]. Quality of the radially polarized light beam can be also improved by transforming the (0, 1)* LG mode with spiral phase and random or uniform polarization and radially (0, 1)* LG mode to nearly-Gaussian beam [26], where the Laguerre-Gaussian (LG) is a ring intensity distribution of radially polarized light. (0, 1)* LG mode with spiral phase and radially (0, 1)* LG mode have different field and phase distributions after this transformation [27]. These two donut modes can be distinguished using the differences in their polarizations and phases. Clear difference between these modes is observed when they pass through a linear polarizer or through the spiral phase element (SPE) [27].

Tunneling ionization that occurs in radially polarized laser field, in the frame of the ADK theory, hasn't been discussed yet, and that's why our research is pointed in that direction. We concentrated our study on analyzing influence of transformed spiral phase and radially (0, 1)* LG mode distributions on tunneling transition rate.

Also, we discussed transition rate when the ionization potential of the ejected electron is not perturbed and when his initial momentum is zero. Additionally, we examine transition rate for nonzero initial momentum and case when perturbation of ponderomotive potential and Stark shift on ionization potential is included. This led us to investigate dependence of the transition rate on the applied field, azimuthal angle ϕ and angle θ, which defines the spiral beam geometry. This study allows us to investigate influence of (0, 1)* Laguerre-Gaussian field distributions on Keldysh parameter and ponderomotive potential of the ejected electron.

This paper is organized as follows, in second chapter we described theoretical background, in chapter three we presented the results and discussed them, and in the final chapter we drew our conclusions. Atomic units are used through this paper ($\hbar = m_e = |e| = 1$).

2. THEORETICAL BECKGKROUND

We begin our study with a brief review of tunnel ionization. In the case of low frequency strong laser field ($I > 10^{14}$ W/cm^2) Coulomb potential becomes perturbed allowing an electron to tunnel. The ionization rate w describes how many ionization processes per unit time occur in constant fields over a period of the external field. The most important atomic and laser properties required to calculate ionization rates are introduced below. The ionization only occurs when an electron receives a certain amount of energy. Since, the energy of all photons is equal and determined by the angular frequency of the laser light, the number of required photons n is:

$$n = \frac{I_p}{\omega} + 1, \tag{1}$$

where I_p is ionization potential, ω photon energy, n is always an integer value.

Ammosov, Delone, and Krainov (ADK) relied on the semiclassical approach and obtained a tunneling ionization rate [8] that increases exponentially with the field strength, without and with initial momentum of ionized electron included [28], respectively:

$$\begin{aligned} w &\propto \exp\left[-\frac{2(2I_p)^{3/2}}{3F}\right], \\ w_p &\propto \exp\left[-\frac{2(2I_p)^{3/2}}{3F} - \frac{p^2\gamma^3}{3\omega}\right], \end{aligned} \tag{2}$$

where p is initial momentum of ionized electron, γ Keldysh parameter, and it has a special form for different laser polarizations: linear, circular and elliptical polarization which will be presented latter.

As it can be seen, ADK tunneling ionization rate depends on the ionization potential I_p, that is equal to the energy at the top of the effective potential barrier, charge of ionized atom Z, but also on laser properties, such as: intensity I and field strength F, the photon energy ω and polarization of laser light. Relation between intensity and field strength is given with equation $I = F^2$.

In the case of the increasing laser intensity or decreasing the photon energy, it comes to $U_p > |I_p| > \omega$, where U_p is ponderomotive potential, and ionization potential of the electron can be changed, enlarged $|I_p| + U_p$. Ponderomotive energy describes the strength of the oscillatory motion of the free electron in an external alternating electric field, it's defined by the expression for linear, circular and elliptical polarization respectively: $U_{p,\mathrm{lin}} = F^2/4\omega^2$, and $U_{p,\mathrm{cir}} = F^2/2\omega^2$, $U_{p,\mathrm{elip}} = (F^2(1-\epsilon^2))/(2\omega^2(1+\epsilon^2))$, value ϵ is ellipticity parameter in the range of (0, 1), for linearly polarized light $\epsilon = 0$, and $\epsilon = \pm 1$, for circularly polarized [29]. This means that ionization can happen only with more photons than usually needed [30]. Also, an energy shift that only exist during the laser pulse duration, the Stark shift, modifies the ground state energy levels and makes the atoms harder to ionize [31]. The ground state is only affected by quadratic Stark shift $\delta E = \alpha F^2/4$ [32], where α is the static polarizability of the atom [33]. Taking all this into account we can represent the effective ionization potential by expression [32]:

$$I_p^{\mathrm{eff}} = I_p + U_p + \delta E. \tag{3}$$

From the Eq. (2) it can be seen that the transition rate is maximum when p, the initial momentum of ejected electron, is zero, so it's expected to decrease with growing p. For our study it is important to analyze

the influence of the initial momentum of ionized electron on the transition rate at the moment immediately after leaving the Coulomb potential barrier. At that moment the electron tunnels out of the atom and moves along a classical trajectory in the laser field, and he feels the influence of both the parent ions and the laser field. It is appropriate to use parabolic coordinates (ξ, η, φ) to describe the motion of this electron [5]. Expression for initial momentum of the electron can be presented by using formula [34]:

$$p(\eta) = (\sqrt{F\eta - 1} + (1/\eta\sqrt{F\eta - 1}))/2, \quad (4)$$

where η is parabolic coordinate. The electron leaves the atom at the point $\eta_{exit} \cong 1/F$, thus the value for η inside the barrier is $1 \ll \eta \ll \eta_{exit}$, while out of the barrier $\eta > \eta_{exit}$ [34]. It is important to emphasize that if the system total energy is independent of the coordinate η, the momentum is conserved along the classical path, i.e. $p_\eta = p$ [5].

Polarization of the laser field has influence on electron ionization process also and we wanted to see if radial polarization offers any advantages over linear or circular polarization when it's used to describe this quantum process and variables that explain it. Theoretical analysis shows that radially polarized beams can be dynamically transform to linearly polarized Gaussian beams, and vice versa [35, 36]. Essential feature that distinguishes these two beams is shape. The radially polarized beams can have donut shape (a zero intensity in the center), otherwise the maximum of intensity of the linearly polarized Gaussian beam occurs in the center. This modification can happen using two modes of radially polarized beam, the LG (0, 1)* spiral-phase mode and the LG (0, 1)* radial-polarization mode. These modes have the same donut shaped intensity distribution, but completely different field distributions. These spatial distributions can be expressed in terms of a coherent superpositions of two orthogonal degenerate LG modes [37, 38] but with a spatially modulated polarization distribution.

The field distribution of the LG (0, 1)* spiral-phase mode is given in form [27]:

$$F_{sp}(r,\phi) = F_0\sqrt{\rho}e^{-\rho/2}e^{\pm i\phi}, \quad (5)$$

where r and ϕ are the cylindrical coordinates, $\rho = 2r^2/R^2$, R is the spot size of the Gaussian beam, $r(\phi) = ae^{k\phi}$ polar equation by which we can describe spiral; a, k are parameters, and the $\pm$ sign depends on the chosen helicity. LG (0, 1)* modes can appear with random or uniform polarization (linear, circular or elliptical) [27, 35].

Specially, electric field distribution of a spiral-phase LG (0, 1)*, for linear and circular polarization is given by Eqs. (6) and (7):

$$F_{sp}^{lin}(r,\phi) = F_0\sqrt{\rho}e^{-\rho/2}e^{-i\phi}(e_x + e_y), \quad (6)$$

$$F_{sp}^{cir}(r,\phi) = F_0\sqrt{\rho}e^{-\rho/2}e^{-i\phi}(e_x + e_y e^{i\pi/2}), \quad (7)$$

where e_x and e_y are the unite vectors along the x and y axis. The electric field for linear polarization becomes:

$$F_{sp}^{lin}(r,\phi) = F_0\sqrt{\rho}e^{-\rho/2}\cos\phi e_x \cdot e_x. \quad (8)$$

For circular right and left hand polarizations electric fields are given with opposite helical index [37]

$$F_{sp}^{cir}(r,\phi) = F_0\sqrt{\rho}e^{-\rho/2}e^{i\phi}(e_x + e_y), \quad (9)$$

$$F_{sp}^{cir}(r,\phi) = F_0\sqrt{\rho}e^{-\rho/2}(e^{-i\phi}e_x - e^{-i\phi}e_y). \quad (10)$$

From the previous equations we can see that distributions, which can display linear and circular forms (in general elliptical), depend only on azimuthal angle ϕ [39].

While the LG (0, 1)* radial-polarization mode field distribution is expressed:

$$F_{rp}(r,\phi) = F_{rp,x}(r,\phi)e_x + F_{rp,y}(r,\phi)e_y, \quad (11)$$

where $\mathbf{e}_x$ and $\mathbf{e}_y$ are unit vectors in the x and y directions, and this mode can be presented with orthogonal linear polarizations and as a superposition of a right hand and left hand circularly polarized mode. Specifically, superposition of right-hand circularly-polarized spiral-phase LG (0, 1)* mode and a left-hand circularly-polarized spiral-phase LG (0, −1)* mode is expressed in form [35, 40, 41]:

$$F_{rp}(r,\phi) = F_0\sqrt{\rho}e^{-\rho/2}[e^{-i\phi}(e_x + e_y e^{i\pi/2}) + e^{i\phi}(e_x + e_y e^{-i\pi/2})] \quad (12)$$

and hence equation has a form:

$$F_{rp}(r,\phi) = 2F_0\sqrt{\rho}e^{-\rho/2}(e_x\cos\phi + e_y\sin\phi). \quad (13)$$

This superposition produces a linearly polarized beam [37]. The corresponding transmitted intensity distribution is calculated as follows [38]:

$$I(r,\phi) = F^*F. \quad (14)$$

At the end of this part and in effort to analyze the tunneling ionization process, we consider influence of effective ionization potential, initial momentum of the ejected electron, and these two field distributions of the LG (0, 1)* modes on transition rate. Thus modified transition rates for the spiral-phase LG (0, 1)* mode and different polarizations are given by expressions [30, 42, 43]:

$$w_{sp,lin} = \frac{F_{sp}^{lin}(r,\phi)D^2}{8\pi Z}\sqrt{\frac{3F_{sp}^{lin}(r,\phi)n^{*3}}{\pi Z^3}} \times\exp\left[-\frac{2(2I_p^{eff})^{3/2}}{3F_{sp}^{lin}(r,\phi)} - \frac{p(\eta)^2\gamma^3}{3\omega}\right], \quad (15)$$

$$w_{sp,cir} = \frac{F_{sp}^{cir}(r,\phi)D^2}{8\pi Z}\exp\left[-\frac{2(2I_p^{eff})^{3/2}}{3F_{sp}^{cir}(r,\phi)} - \frac{p(\eta)^2\gamma^3}{3\omega}\right], \quad (16)$$

$$w_{\mathrm{sp,elip}} = \sqrt{\frac{3}{\pi}\frac{1}{(1-\epsilon^2)}\frac{F_{\mathrm{sp}}^{\mathrm{cir}}(r,\phi)}{(2I_p^{\mathrm{eff}})^{3/2}}}\frac{F_{\mathrm{sp}}^{\mathrm{cir}}(r,\phi)D^2}{8\pi Z} \times \exp\left[-\frac{2(2I_p^{\mathrm{eff}})^{3/2}}{3F_{\mathrm{sp}}^{\mathrm{cir}}(r,\phi)} - \frac{p(\eta)^2\gamma^3}{3\omega}\right], \quad (17)$$

where $n^* = Z/\sqrt{2I_p}$ is effective principal quantum number of the ionized state, F^{lin} is field strength for linear and F^{cir} for circular polarization of laser light, I is laser intensity and $D = \left(\frac{4Z^3}{Fn^{*4}}\right)^{n^*}$. Variables n^* and D are also adapted.

For radial-polarization LG (0, 1)* mode will be used modified transition rates for linear polarization with variables proper to this case.

3. RESULTS AND DISCUSSION

Ionization of one electron would break the stable electronic configuration and we want to see by which intensity of the laser field will it have the ability to tunnel. Ionization potential for the first electron in valence shell of Ar atom is $I_p = 0.5791$ in atomic units, so the charge of the ionized system is $Z = 1$. Tunneling transition rate is sensitive to laser frequency, that's why our choice was Ti:Sapphire laser with wavelength $\lambda = 800$ nm and in this case the photon energy is $\omega = 0.5696$, while the field strengths for linear and circular polarization are given by expressions: $F_{\mathrm{lin}} = 5.4 \times 10^{-9}\sqrt{I}$, $F_{\mathrm{cir}} = 3.7 \times 10^{-9}\sqrt{I}$ in atomic units.

Next step is to investigate field distributions of two radially polarized (LG) (0, 1)* modes, LG (0, 1)* spiral-phase and LG (0, 1)* radial-polarization field distributions, on the tunneling transition rate. A radial polarized beam can be used to produce a much smaller focused spot than a conventional linear or circular polarized beam can produce [44, 45]. Laser beam spot size can be of the order of millimeters (15–30 mm), but also of micrometers (3–60 μm). We accepted that beam diameter is fixed to the value 3 μm (5.7×10^4 in atomic unit). Also, it was necessary to define the parameters that determine the logarithmic function $r(\phi) = ae^{k\phi}$, where $a = 0.57$ (1.08×10^4 in a.u.) when r is in μm. The constant $k = \tan\theta$. Angle θ defines spiral geometry and can take value in range of [–90°, 90°]. For $\theta = 22.5°$ and $\theta = 45°$ are $k = 0.414$ and $k = 1.0$, and for every other value of the angle θ in given range is calculated in this way [38].

Through our work we want to show that behavior of essential physical quantities can be analyzed using different modes in a wide range of laser field intensities.

At the beginning of discussion in the Figs. 1–4 it's shown behavior of the transition rate with the LG (0, 1)* spiral-phase field distribution without additional effects included.

In Fig. 1 we presented the influence of azimuthal angle on the transition rate. As we can see azimuthal angle has very small influence until the angles of 40°. This theoretical approach limits us to compute transition rate for azimuthal angles of <50°. In case of $\phi = 20°$ transition rate has approximately maximum value around laser intensity of $I = 8 \times 10^{17}$ W/cm^2. Thereafter with increasing angle the transition rate slowly decreases. Considering that azimuthal angle ϕ lie in an interval span of 360°, or [–180°, +180°], we test the transition rate dependence when the azimuthal angle is negative. In contrast to the positive angle, for the azimuthal negative angle, the transition rate decreases rapidly as we move away in the negative direction. Figure 2 shows that transition rate has similar dependence as in previous case, with slightly lower magnitude. The LG (0, 1)* spiral-phase field distribution determine limiting angle we can use in this commutation (in this case –35°).

The graphs in Fig. 3 show calculation performed for linearly polarized laser field with the LG (0, 1)* spiral-phase field distribution for fixed laser intensity and an azimuthal angle that changes in an interval [0, 45°]. All panes of Fig. 3 demonstrate that curve has maximum on the angle of $\phi = 30°$, except for the intensity of the laser field at 10^{18} W/cm^2, where the transition rate is equal to zero for this angle. On this intensity we can observe that two maxima of the transition rate occur at angles of $\phi = 4.4°$ and $\phi = 43°$. We can see that with decreasing laser field intensity, the maximum of transition rate declines. The range of the angles, at which tunnel ionization occurs, narrows. This is caused by low perturbation atomic levels due to low laser field intensity.

To complete our analysis, we examine dependence of the pure transition rate (without included effects) with the LG (0, 1)* spiral-phase field distribution on the θ angle, which defines the spiral beam geometry. For angles of $\theta = 0°$ and 90° radial and azimuthal polarized plane waves can be generated, respectively. Also, at intermediate angles a series of highly interesting spirals can be created [38]. Hence, we limited our analysis to angles from 0° to close to 90° (Fig. 4). It can be seen that as the value of θ increases, the transition rate increases too. Angle $\theta = 90°$ gives pure azimuthal polarized wave, therefore is not included in our computation.

The next discussion expands the previous analysis by including additional effects in the transition rate. The three transition rates were obtained with the LG (0, 1)* spiral-phase field distribution beams that were polarized linearly, circularly and elliptically. These transition rates are given in Figs. 5, 8, 9 with intensity in the range of 1×10^{14}–5×10^{17} W/cm^2. Besides the ionization transition rate depends on laser intensity, it also has dependences on initial momentum of ejected electron, ponderomotive potential and Stark shift.

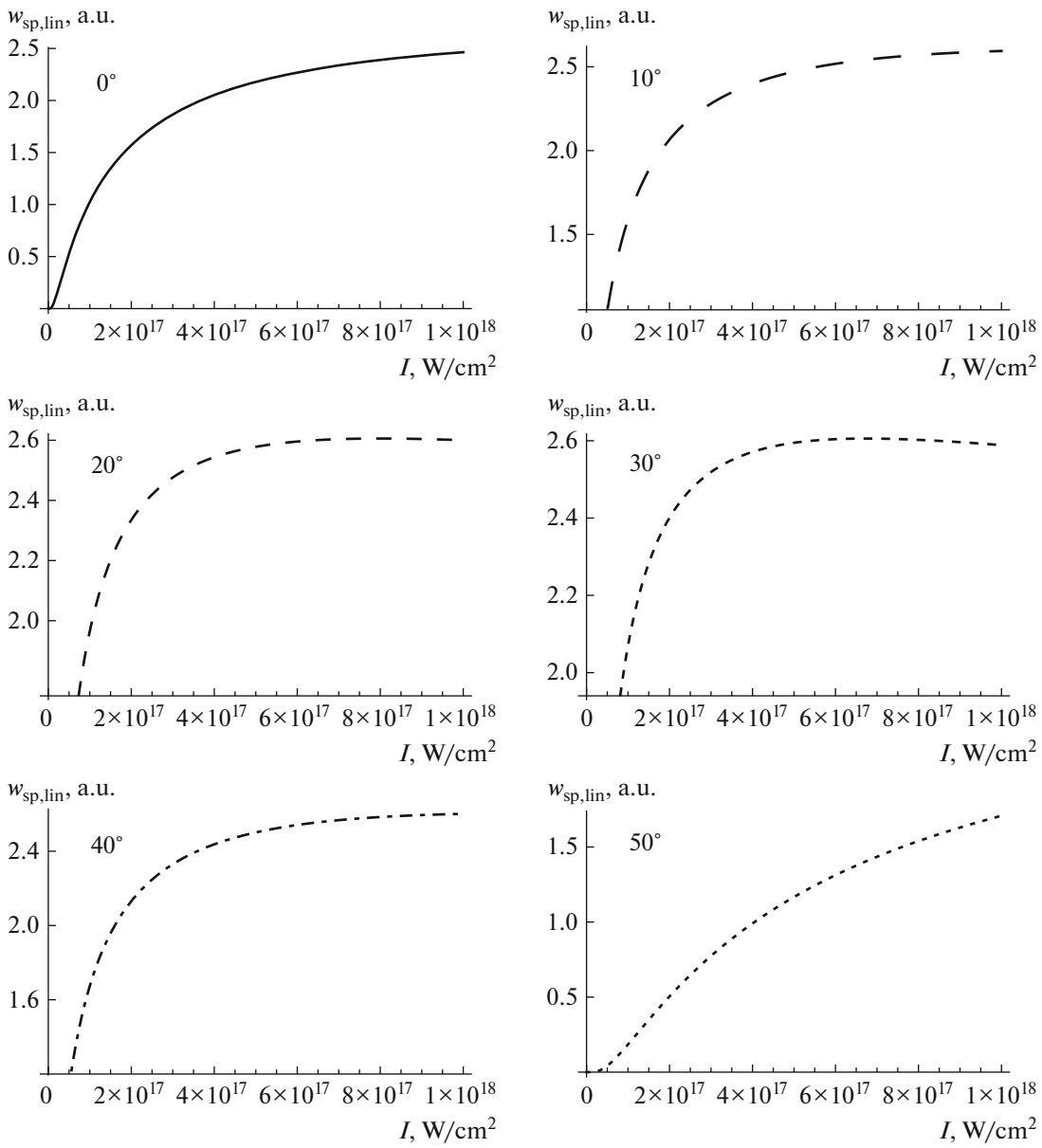

Fig. 1. Transition rate (in arbitrary units [a.u.]) for linear polarized laser field with the LG (0, 1)* spiral-phase field distribution in function of laser intensity for azimuthal angle.

According to perturbation theory, the shift of a level is determined by the vibrational energy of the free electron in the field. At large field strengths F and small frequency ω, the shift can be very large, also Stark shift of a highly excited level may exceed unperturbed binding energy of electron. Ionization rates decrease due to these effects, first with the inclusion of ponderomotor potential and then slightly with the inclusion of the Stark effect, so the following obtained graphs are partially expected.

Using the LG (0, 1)* spiral-phase mode of radially polarized beam gives a result such that two maximums (two peaks) are noticed, while the transition rate that was analyzed in earlier studies, would show only one peak.

On the first peak (left peak, the one at lower laser intensities) the order of the transition rates curves' maximums' intensities is opposite than the order of a second expected peak (right peak, the one at higher laser intensities) curves. Peaks occur at intensities 2.17×10^{16} and 7.81×10^{16} W/cm^2. We suppose that this behavior is affected by atomic core since point of electron exit is closer than in case of high values of η.

Analyzing the obtained results, in frame of the LG (0, 1)* spiral phase mode in case of linear polarization, the inclusion of the initial momentum of ejected elec-

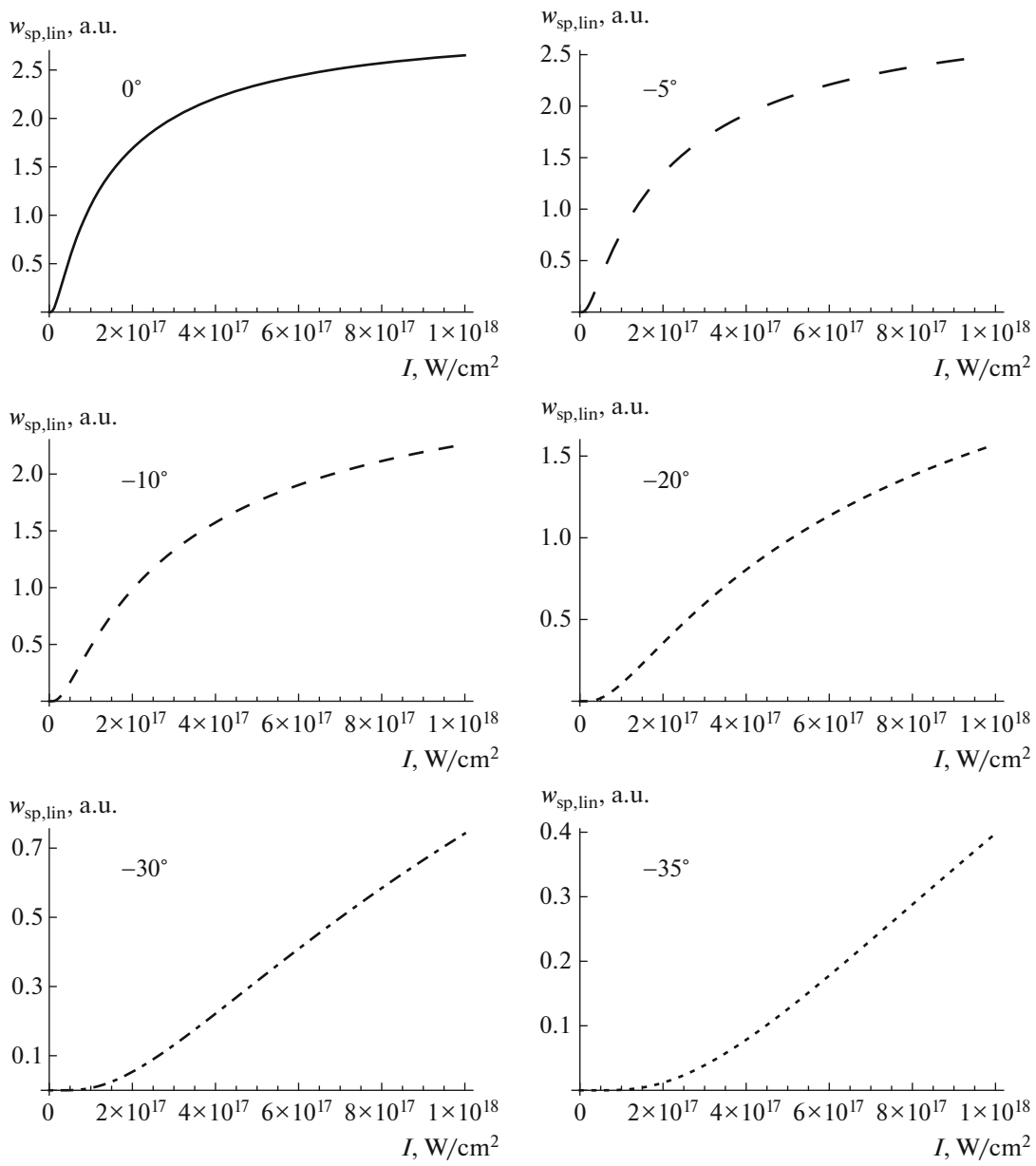

Fig. 2. Transition rate (in arbitrary units (a.u.)) for linear polarized laser field with the LG (0, 1)* spiral-phase field distribution in function of laser intensity for fixed negative azimuthal angle.

tron gives a more complex dependence of the transition rate curve on the laser field intensity. With a certain set of parameters, and for smaller values of the coordinate $\eta < 10$, which represents the point of the electron's exit from the barrier, the second term of the momentum (Eq. (4)) leads to the appearance of two transition rate peaks, probably due to the influence of the core and the electronic envelope (non-uniform field distribution) on ejected electron leads to a violation of continuity transition rate.

Observed the left peak gives a non-zero transition rate, and shows that with the inclusion of the effects, the transition rate will be higher, which is a conclusion that needs to be confirmed experimentally.

It can also be seen that with an increase of the coordinate η, the second term in the momentum equation decreases, which leads to decreasing of the left peak. Position of the peak is also determined by the reciprocal dependence of the momentum on the field strength also in this term.

A more detailed study showed that at the lower values of the η coordinate two peaks appear, while at higher values of this coordinate the two peaks overlap (only one appears) (Fig. 6).

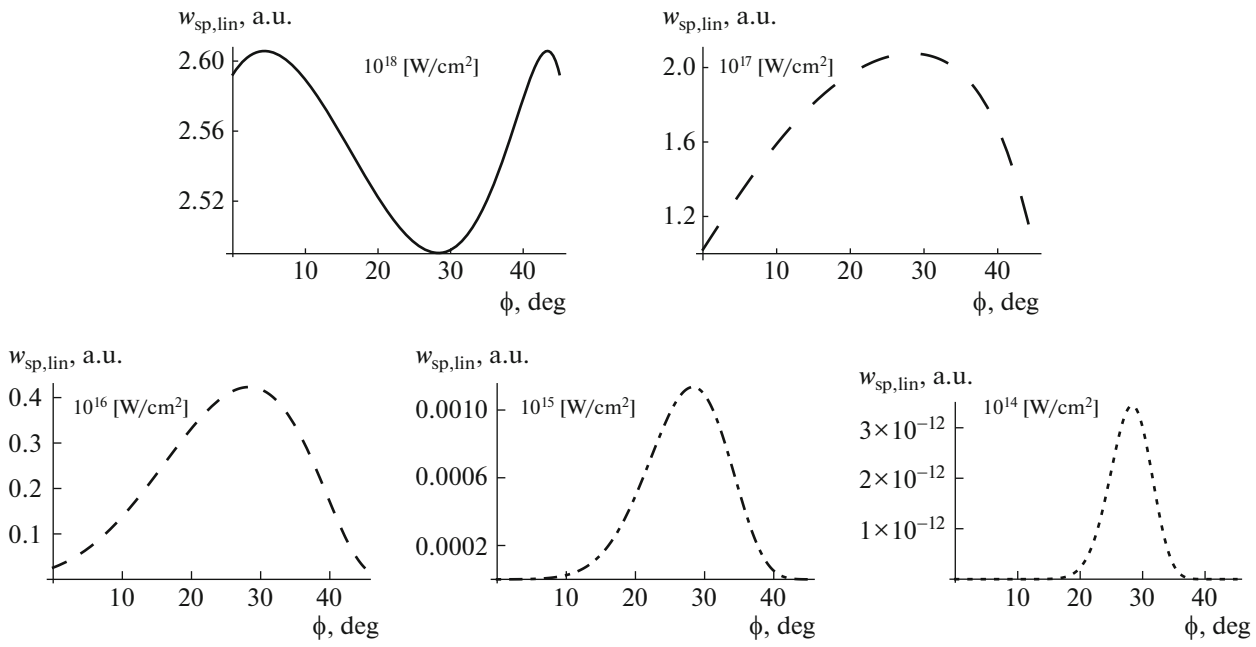

Fig. 3. Transition rate (in arbitrary units [a.u.]) for linear polarized laser field with the LG (0, 1)* spiral-phase field distribution in function of azimuthal angle for fixed laser intensity.

We want to emphasize how the transition rate moves towards lower intensities of the laser field with increasing η (Figs. 6, 7). It can be noticed that for η = 100, the maximum transition rates are at intensities of $I \sim 10^{14}$, which is in full accordance with our previous works [28].

In Figs. 8 and 9 are presented transition rates for elliptically polarized laser field and circularly polarized laser field as a special case of elliptically polarization, respectively. Using these types of polarizations, two peaks on the graph were obtained too, and the maximums occur at same intensities of laser fields 2.31×10^{16} and 7.11×10^{17} W/cm^2.

Observing these two figures, it is noticeable that in addition to the above similarities, one can clearly see the difference in the values of the transition rates. The transition rates at field intensity $I = 2.31 \times 10^{16}$ W/cm^2 (left peak) have a higher value when the atom is in a circularly polarized field.

To get a clearer picture of the transition rate behavior, we gave it's dependence on the laser field intensity and azimuthal angle on 3D graph (Fig. 10).

As can be seen, the dependence is complex. The transition rate does not increase constantly with increasing azimuthal angle value and with increasing field. It is noticed that for certain values of laser intensity with increasing azimuthal angle ϕ up to 15 deg the transition rate increases, in the interval from 15 to 35 deg the value of the transition rate approaches zero and then with further increase of the azimuthal angle the transition rate increases again.

Finally, in order to discuss the influence of the LG (0, 1)* spiral-phase mode on the parameters that directly affect the transition rate in detail, it is important to analyze Keldysh parameter and ponderomotive potential (Figs. 11, 12).

To observe the behavior of the Keldysh parameter we presented it by the equation $\gamma = \omega(\sqrt{2I_p}/F)$, which clearly shows the influence of the effective ionization potential I_p^{eff} and the laser field distribution F on this

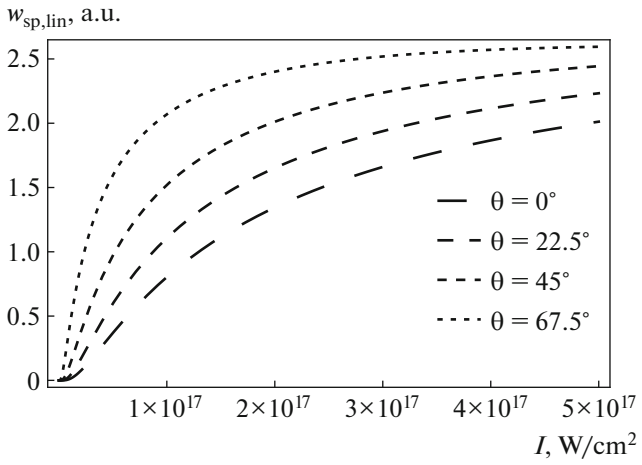

Fig. 4. Transition ionization rate for linear polarized laser field with the LG (0, 1)* spiral-phase field distribution in function of laser intensity and for three different values of angle θ.

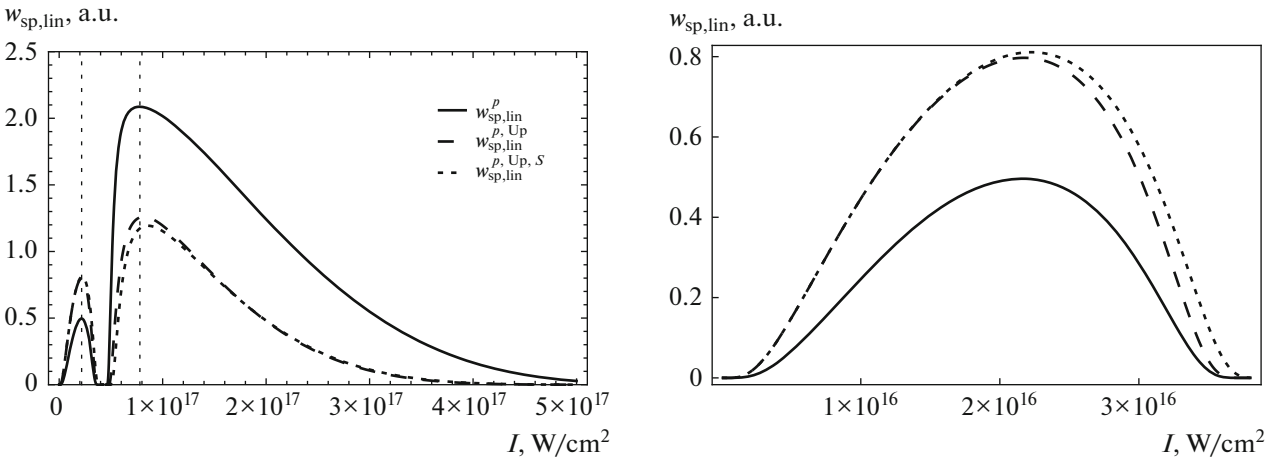

Fig. 5. Transition ionization rate in linearly polarized laser field with the LG (0, 1)* spiral-phase field distribution and with effects included (left pane). Right pane shows highlighted left peak.

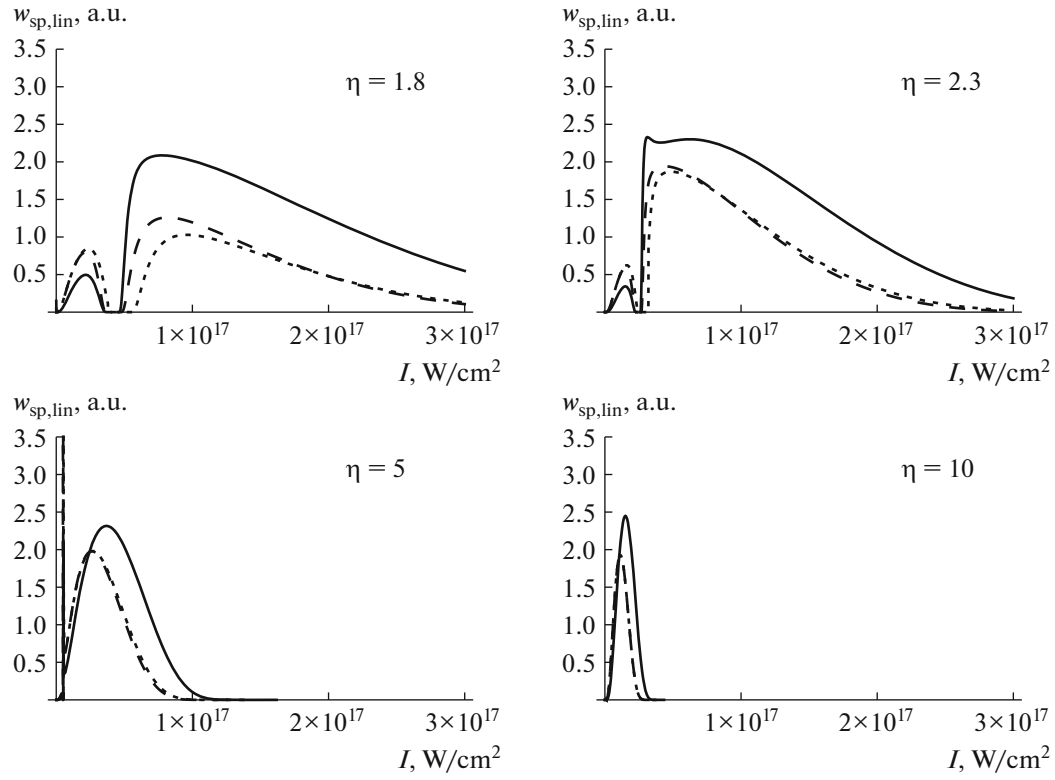

Fig. 6. Transition ionization rate in linearly polarized laser field with the LG (0, 1)* spiral-phase field distribution for different η coordinate values, where $w^{p}_{sp,lin}$ is shown by black solid line, $w^{p,U_p}_{sp,lin}$ with dashed line and $w^{p,U_p,S}_{sp,lin}$ with dotted line.

parameter. As we can see, the curves describing the behavior of the Keldysh parameter in the ordinary linear and circular field distributions, as well as the Keldysh parameter in these polarization with field distribution in the LG (0, 1)* spiral-phase mode, have an exponential decrease with increasing laser field intensity. Also, it is obtained that the more dominant influence of the LG (0, 1)* spiral-phase mode on this parameter is in the linearly polarized field (Fig. 11).

Affect of the LG (0, 1)* spiral-phase mode on ponderomotive potential is also taken into account (Fig. 12). We analyzed the ponderomotive potential in a linear, circular, and elliptical polarized laser field, with and without LG (0, 1)* spiral-phase field distri-

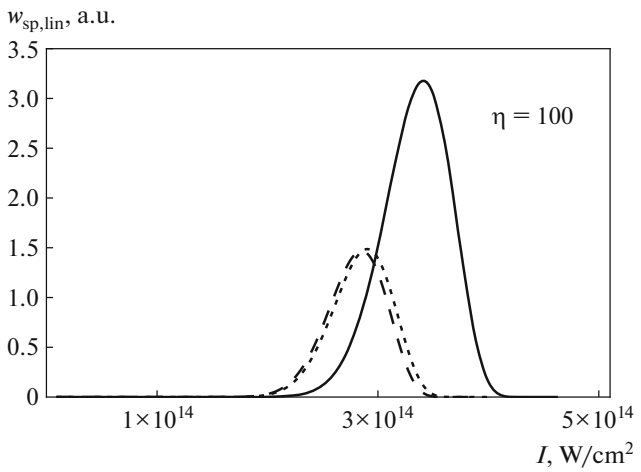

Fig. 7. Transition ionization rate in linearly polarized laser field with the LG (0, 1)* spiral-phase field distribution at $\eta = 100$, where $w^{p}_{sp,lin}$ is shown by black solid line, $w^{p,U_p}_{sp,lin}$ with dashed line and $w^{p,U_p,S}_{sp,lin}$ with dotted line.

bution included. Depending on the LG (0, 1)* spiral-phase mode presence, with the same parameter sets, the curves' orders are different. Ponderomotive potential has a lower value in the application of the LG (0, 1)* field distribution and the greatest influence is observed for $U_{p,\,lin}$.

In intention to analyze the behavior of the transition ionization rate in detail, we complemented this discussion by giving brief insight into it's behavior and parameters that determine it, for a given atom in the LG (0, 1)* radial-polarization mode.

Based on Eq. (16), we obtained the transition rate for a circularly polarized laser field for the LG (0, 1)* radial-polarization mode field distribution as a special case of an elliptically polarized laser field. The way of acting of this transition rate for different values of the ellipticity parameter ϵ was observed, too. It was shown that the ellipticity ϵ, taking it in the interval from 0 to 1, has no effect on the transition rate.

To broaden the previous discussion, in the following figures will be presented the Keldysh parameter and ponderomotive potential within the LG (0, 1)* radial-polarization mode field distribution depending on laser intensity.

When the value of azimuthal angle at $\phi = \pi/6$ is fixed and the laser intensity increases, from Fig. 14 it can be seen that Keldysh parameter for the ordinary circular laser field distribution and the LG (0, 1)* radial-polarization field distribution have different values. With an increase in the intensity of the laser field, the value of the Keldysh parameter decreases and the distance between γ_{cir} and $\gamma_{rad,cir}$ curves for the fixed value of the laser field intensity is different.

Ponderomotive potential changes when the LG (0, 1)* radial-polarization field distribution is added to it. Obtained curves are illustrated in Fig. 15. As in the case of the LG (0, 1)* spiral-phase mode, the inclusion of the LG (0, 1)* radial-polarization field distribution leads to an increase in the ponderomotive potential.

4. CONCLUSIONS

Tunnel ionization for atomic target of an argon in strong field regime is discussed. We developed the idea to analyze dependence of tunneling transition rate on initial momentum and transformed ionization potential (inclusion of Stark shift and ponderomotive potential) when field distribution is given by radially polarized donut (0, 1)* Laguerre–Gaussian beam.

We present behavior of the transition rate without additional effects included in linearly polarized laser

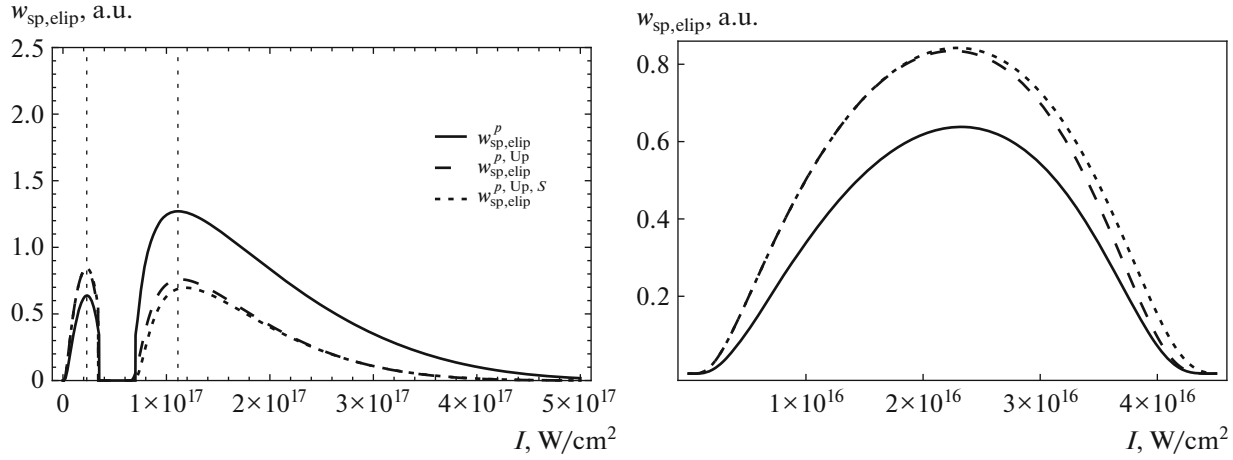

Fig. 8. Transition ionization rates in elliptically polarized laser field with the LG (0, 1)* spiral-phase field distribution and with effects included (left pane). Right pane shows highlighted left peak.

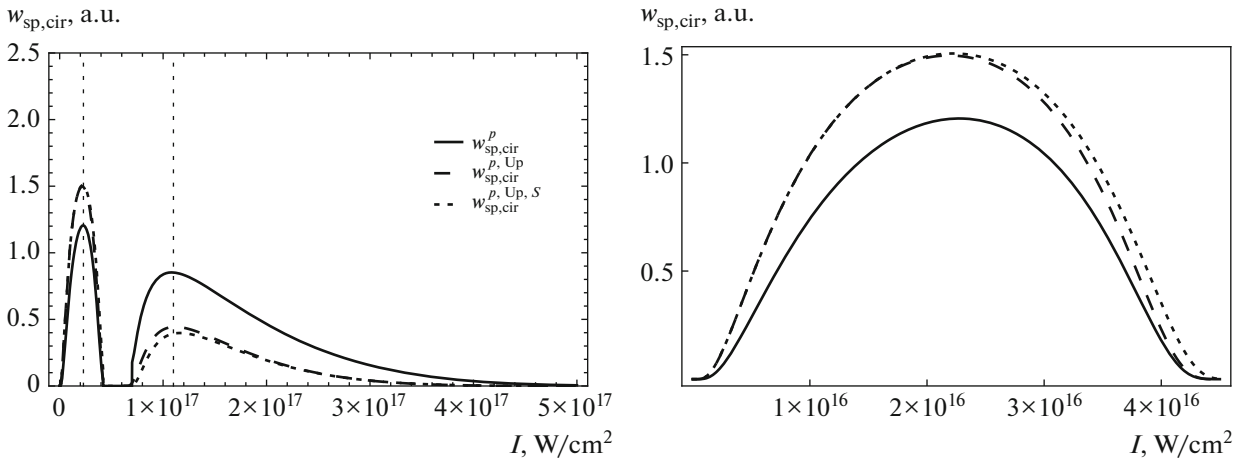

Fig. 9. Transition ionization rates in circularly polarized laser field with the LG (0, 1)* spiral-phase field distribution and with effects included (left pane). Right pane shows highlighted left peak.

field with the LG (0, 1)* spiral-phase field distribution, for fixed values of the azimuthal angle in a function of laser intensity and vice verse, as well as its dependence on the spiral geometry of the beam (θ angle). In further discussion we observed how the inclusion of additional effects influence the behavior of the transition rate when the laser field is linearly, circularly and elliptically polarized with the LG (0, 1)* spiral-phase field distribution. We have also compared the way the Keldysh parameter and ponderomotive potential behave in linearly and circularly polarized laser field without concretizing the field distribution and with LG (0, 1)* spiral-phase field distribution.

From this research we derive major conclusions:

— The transition rate is affected by a change in the azimuthal angle. For angle values in the range from $\varphi = 0°$, to $\varphi = 40°$, the transition rate increases and then decreases slightly. A visible change or decrease is observed at an angle of $\varphi = 50°$. Changes in transition rate are more noticeable for negative azimuthal angles. Transition rate decrease constantly for angles $\varphi = -5°$, $-10°$, $-20°$, $-30°$ in such a way that for the $\varphi = -35°$ it has about six times less value than for the $\varphi = 0°$.

— In the case when we fixed the laser intensity and changed the angle φ we noticed the appearance of two peaks on intensity at 10^{18} W/cm^2, and then as intensity decrease one peak disappears and transition rate curve narrows.

— We have also shown that the spiral beam geometry affects the transition rate. Is clearly evident, as the angle increases, so does the rate of transition.

— In case of linear polarized field, we obtained that the transition rate splits into two peaks that are quite close localized. Occurrence and the position of the two peaks has relationship with the inclusion of the initial momentum of the ejected electron in the equation for the transition rate and the manner in which the initial momentum of the ejected electron depends on the η coordinate and the field strength. We have shown that with increasing η second peak disappears and transition rate shifts to lower intensities of the laser field.

— For an elliptically polarized laser field as well as a circular one we can notice occurrence of two peaks. In linear and elliptical polarization, the first peaks have maxima at low value, but in the case of circular polarization first peak has higher value.

—Additionally, we presented the influence of the LG (0, 1)* spiral-phase field distribution on the Keldysh parameter and ponderomotive potential is opposite, while the Keldysh parameter increases, the inclusion of the LG (0, 1)* spiral-phase field distribution leads to a decrease in ponderomotive potential which is most pronounced in the case of linear polarization.

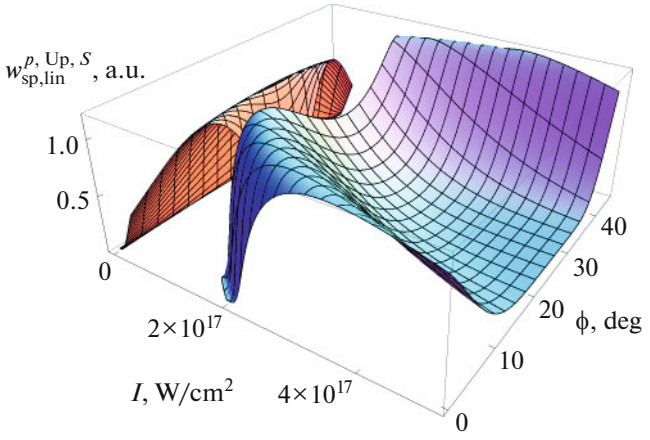

Fig. 10. 3D graph of transition ionization rate with the LG (0, 1)* spiral-phase field distribution in the function of laser intensity I and azimuthal angle ϕ.

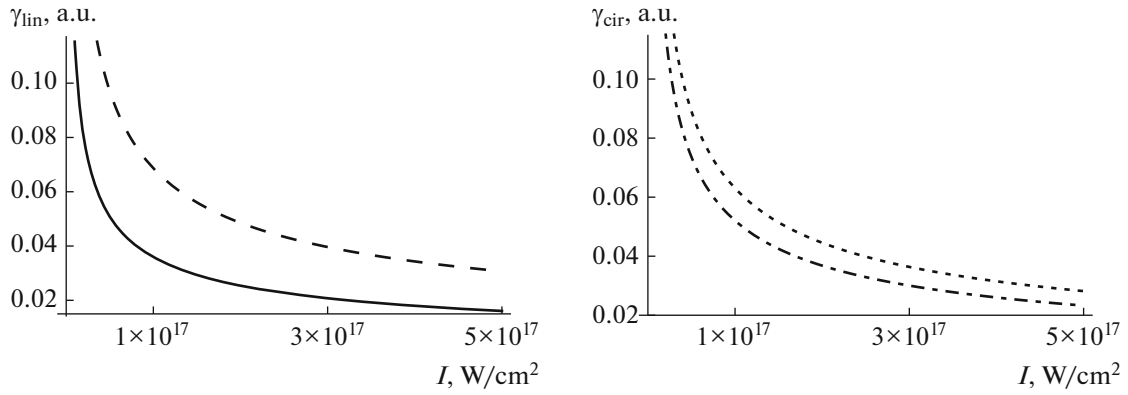

Fig. 11. Keldysh parameter in linearly polarized laser field (left pane) and in circularly (right pane) with the LG (0, 1)* spiral-phase field distribution, in the function of laser intensity in range $I = (10^{14}–5 \times 10^{17})$ W/cm^2 and fixed value of azimuthal angle at $\phi = \pi/6$. The curves in the figure are represented as follows: γ_{lin}-black solid line, $\gamma_{sp,\,lin}$-dashed line, γ_{cir}-dash-dotted line, $\gamma_{sp,\,cir}$-dotted line.

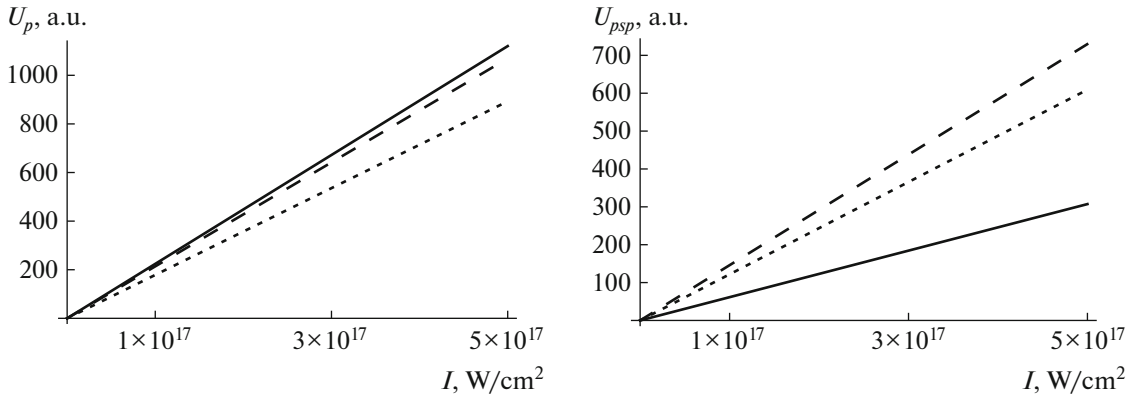

Fig. 12. Ponderomotive potential (left pane) and ponderomotive potential with the LG (0, 1)* spiral-phase mode field distribution included (right pane), in the function of laser intensity in range $I = (10^{14}–5 \times 10^{17})$ W/cm^2 and fixed values of azimuthal angle at $\phi = \pi/6$ and ellipticity $\epsilon = 0.3$.The curves in the figure are represented as follows: $U_{p,\,lin}$-black solid line, $U_{p,\,cir}$-dashed line, $U_{p,\,elip}$-dotted line.

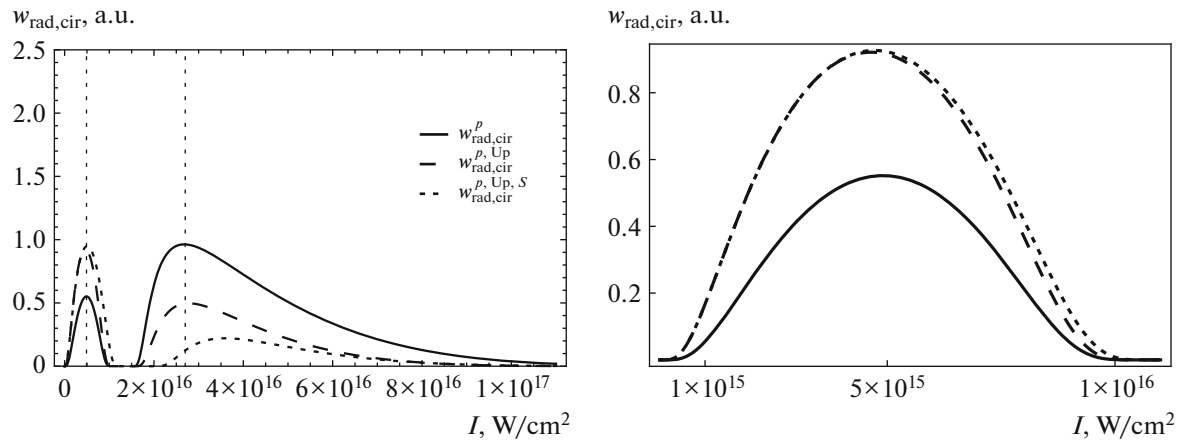

Fig. 13. Transition ionization rate in circularly polarized laser field with the LG (0,1)* radial-polarization mode field distribution and with effects included (left pane). Right pane shows highlighted left peak.

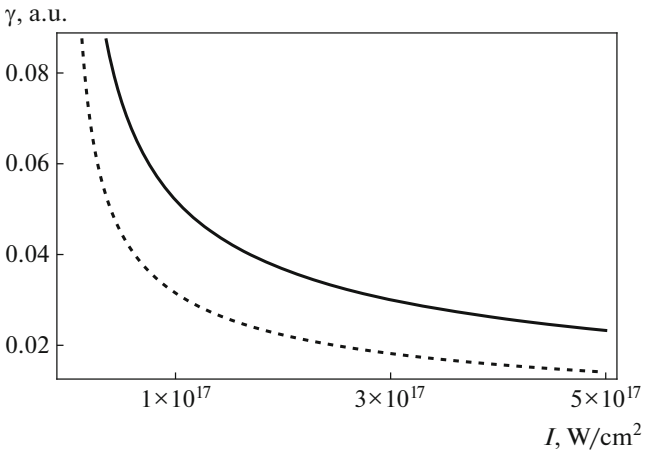

Fig. 14. Keldysh parameter in circularly polarized laser field with the LG (0, 1)* radial-polarization field distribution, in the function of laser intensity in range $I = (10^{14}–5 \times 10^{17})$ W/cm^2 and fixed value of azimuthal angle at $\phi = \pi/6$. The curves in the figure are represented as follows: γ_{cir}-black solid line, $\gamma_{rad,\ cir}$-dotted line.

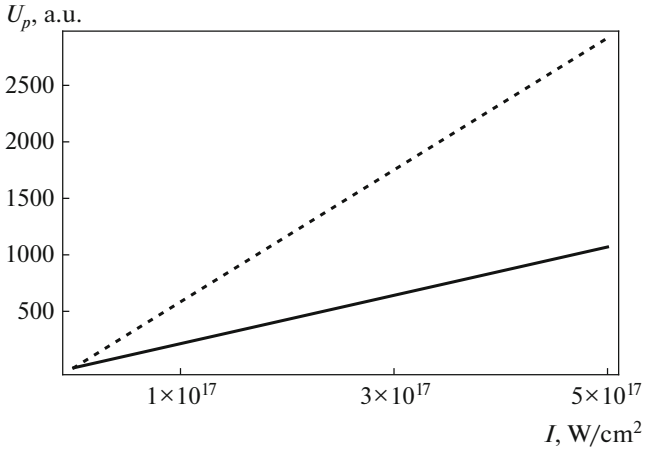

Fig. 15. Ponderomotive potential in circularly polarized laser field with the LG (0, 1)* radial-polarization field distribution, in the function of laser intensity in range $I = (10^{14}– U_{p,\ cir}5 \times 10^{17})$ W/cm^2 and fixed value of azimuthal angle at $\phi = \pi/6$. The curves in the figure are represented as follows: $U_{p,\ cir}$-black solid line, $U_{p,\ rad,\ cir}$-dotted line.

— At the very end, we have briefly shown that the inclusion of the LG (0, 1)* radial-polarization field distribution has an influence on the behavior of the transition rate, the Keldysh parameter and the ponderomotive potential in the same way as the inclusion of the spiral mode.

We can conclude that there is a wide range of laser intensities, field distributions and polarizations of laser light under which the ionization process of an atom can be analyzed. The appearance of the two peaks contains important information about the ionization process so that the transition rate is affected by all the additional effects involved and it should be of interest to continuations of this work to improve this theory and verify the obtained results in experiment.

ACKNOWLEDGMENTS

The authors acknowledge funding provided by the University of Kragujevac - Institute for Information Technologies (the contract 451-03-68/2020-14/200378), University of Kragujevac - Faculty of Science (the contract 451-03-68/2020-14/200122) through the grants by the Ministry of Education, Science and Technological Development of the Republic of Serbia.

REFERENCES

1. N. I. Shvetsov-Shilovski, D. Dimitrovski, and L. B. Madsen, Phys. Rev. A **85**, 023428 (2012).
2. J. E. Calvert, Han Xu, A. J. Palmer, et al., Sci. Rep. **6**, 34101 (2016).
3. Y. H. Lai, J. Xu, U. B. Szafruga, et al., Phys. Rev. A **96**, 063417 (2017)
4. N. I. Shvetsov-Shilovski, M. Lein, and K. Tökési, Eur. Phys. J. D **73**, 37 (2019).
5. L. D. Landau and E. M. Lifshitz, *Course of Theoretical Physics*, Vol. 3: *Quantum Mechanics: Non-Relativistic Theory* (Nauka, Moscow, 1989, 4th ed.; Pergamon, New York, 1977, 3rd ed.).
6. L.V. Keldysh, Sov. Phys. JETP **20**, 1307 (1965).
7. A. M. Perelomov, V. S. Popov, and M. V. Terent'ev, Sov. Phys. JETP **23**, 924 (1966).
8. V. M. Ammosov, N. B. Delone, and V. P. Krainov, Sov. Phys. JETP **64**, 1191 (1986).
9. V. S. Popov, J. Exp. Theor. Phys. **91**, 48 (2000).
10. C. L. Wang, X. Y. Lai, Z. L. Hu, et al., Phys. Rev. A **90**, 013422 (2014).
11. M. Yuan, P. P. Xin, T. S. Chu, and H. P. Liu, Opt. Express **25**, 23493 (2017).
12. J. Cai, Y. J. Chen, Q. Z. Xia, et al., Phys. Rev. A **96**, 033413 (2017).
13. R. Wang, Q. Zhang, D. Li, et al., Opt. Express **27**, 6471 (2019).
14. M. Lein, J. Mod. Opt. **58**, 1188 (2011).
15. D. G. Arbó, C. Lemell, and J. Burgdörfer, J. Phys.: Conf. Ser. **635**, 012003 (2015).
16. W. Quan, M. Yuan, S. Yu, et al., Opt. Express **24**, 23248 (2016)
17. A. S. Stodolna, F. Lépine, T. Bergeman, et al., Phys. Rev. Lett. **113**, 103002 (2014).
18. H. Moradi, V. Shahabadi, E. Madadi, et al., Opt. Express **27**, 7266 (2019).
19. M. Kaur and D. N. Gupta, IEEE Trans. Plasma Sci. **45**, 2841 (2017).
20. Y. Kozawa, T. Hibi, A. Sato, et al., Opt. Express **19**, 15947 (2011).

21. C. Hnatovsky, V. G. Shvedov, and W. Krolikowski, Opt. Express **21**, 12651 (2013).
22. S. Quabis, R. Dorn, M. Eberler, et al., Opt. Commun. **179**, 1 (2000).
23. I. Moshe, S. Jackel, Y. Lumer, et al., in *Proceedings of the CLEO/Europe and EQEC 2011 Conference, OSA Technical Digest (CD)* (Optical Society of America, 2011), paper CA9_5.
24. T. L. Jefferson-Brain, C. R. Smith, M. D. Burns, et al., Appl. Phys. B **125**, 167 (2019).
25. Y. Ma, Opt. Rev. **19**, 39 (2012).
26. R. Oron, N. Davidson, A. A. Friesem, and E. Hasman, Opt. Lett. **25**, 939 (2000).
27. G. Machavariani, Y. Lumer, I. Moshe, and S. Jackel, Opt. Commun. **271**, 190 (2007).
28. V. M. Ristić, T. B. Miladinović, and M. M. Radulović, Laser Phys. **18**, 1183 (2008).
29. H. R. Reiss, Phys. Rev. Lett. **101**, 043002 (2008).
30. N. B. Delone and V. P. Krainov, Phys. Usp. **41**, 469 (1998).
31. N. B. Delone and V. P. Krainov, Phys. Usp. **42**, 669 (1999).
32. E. A. Volkova, A. M. Popov, and O. V. Tikhonova, J. Exp. Theor. Phys. **113**, 394 (2011).
33. J. Mitroy, M. S. Safronova, and Ch. W. Clark, J. Phys. B: At., Mol. Opt. Phys. **43**, 20201 (2010).
34. D. Bauer, *Theory of Laser–Matter Interaction* (Max-Planck Inst., Heidelberg, 2002).
35. G. Machavariani, N. Davidson, Y. Lumer, et al., in *Proceedings of the 2007 European Conference on Lasers and Electro-Optics and the International Quantum Electronics Conference, Munich, 2007*, p. 1.
36. D. J. Armstrong, M. C. Phillips, and A. V. Smith, Appl. Opt. **42**, 3550 (2003).
37. C. Maurer, A. Jesacher, S. Fürhapter, et al., New J. Phys. **9**, 78 (2007).
38. J. Ouyang, W. Perrie, O. J. Allegre, et al., Opt. Express **23**, 12562 (2015).
39. V. E. Lembessis and M. Babiker, Phys. Rev. A **81**, 033811 (2010).
40. J. Courtial, D. A. Robertson, K. Dholakia, et al., Phys. Rev. Lett. **81**, 4828 (1998).
41. S. Vyas, Y. Kozawa, and Y. Miyamoto, Opt. Express **23**, 33970 (2015).
42. N. B. Delone and V. P. Krainov, *Multiphoton Processes in Atoms* (Springer, Berlin, 2000).
43. C. Z. Bisgaard and L. B. Madsen, Am. J. Phys. **72**, 249 (2004).
44. R. Dorn, S. Quabis, and G. Leuchs, Phys. Rev. Lett. **91**, 233901 (2003).
45. K. M. Tanvir Ahmmed, C. Grambow, and A. M. Kietzig, Micromachines **5**, 1219 (2014).